# Observational Study of Wind Channeling within the St. Lawrence River Valley

MARCO L. CARRERA,* JOHN R. GYAKUM, AND CHARLES A. LIN*

*McGill University, Montreal, Quebec, Canada*

(Manuscript received 19 June 2008, in final form 13 January 2009)

ABSTRACT

The presence of orography can lead to thermally and dynamically induced mesoscale wind fields. The phenomenon of channeling refers to the tendency for the winds within a valley to blow more or less parallel to the valley axis for a variety of wind directions above ridge height. Channeling of surface winds has been observed in several regions of the world, including the upper Rhine Valley of Germany, the mountainous terrain near Basel, Switzerland, and the Tennessee and Hudson River Valleys in the United States. The St. Lawrence River valley (SLRV) is a primary topographic feature of eastern Canada, extending in a southwest–northeast direction from Lake Ontario, past Montreal (YUL) and Quebec City (YQB), and terminating in the Gulf of St. Lawrence. In this study the authors examine the long-term surface wind climatology of the SLRV and Lake Champlain Valley (LCV) as represented by hourly surface winds at Montreal, Quebec City, and Burlington, Vermont (BTV). Surface wind channeling is found to be prominent at all three locations with strong bidirectionalities that vary seasonally. To assess the importance of the various channeling mechanisms the authors compared the joint frequency distributions of surface wind directions versus 925-hPa geostrophic wind directions with those obtained from conceptual models. At YUL, downward momentum transport is important for geostrophic wind directions ranging from 240° to 340°. Pressure-driven channeling is the dominant mechanism producing northeasterly surface winds at YUL. These northeasterlies are most prominent in the winter, spring, and autumn seasons. At YQB, pressure-driven channeling is the dominant physical mechanism producing channeling of surface winds throughout all seasons. Of particular importance, both YUL and YQB exhibit countercurrents whereby the velocity component of the wind within the valley is opposite to the component above the valley. Forced channeling was found to be prominent at BTV, with evidence of diurnal thermal forcing during the summer season. Reasons for the predominance of pressure-driven channeling at YUL and YQB and forced channeling at BTV are discussed.

## 1. Introduction

The presence of orography can lead to thermally and dynamically induced mesoscale wind fields (Whiteman and Doran 1993; Weber and Kaufmann 1998; Rampanelli et al. 2004; Drobinski et al. 2007; Mayr et al. 2007; Zhong et al. 2008). The phenomenon of channeling refers to the tendency for the winds within a valley to blow more or less parallel to the valley axis for a variety of wind directions above ridge height (Eckman 1998; Weber and Kaufmann 1998; Kossmann and Sturman 2003; Nawri and Stewart 2006, 2008). Channeling of surface winds has been observed in several regions of the world, including the upper Rhine Valley of Germany (Gross and Wippermann 1987), the mountainous terrain near Basel, Switzerland (Weber and Kaufmann 1998), the Tennessee (Whiteman and Doran 1993; Eckman 1998) and Hudson Valleys (Fitzjarrald and Lala 1989) in the United States, and the eastern Canadian Arctic (Nawri and Stewart 2006, 2008).

Whiteman and Doran (1993) discuss conceptual models for four different physical mechanisms to account for the relationship between the synoptic, or above-valley, winds and the winds within the valley. The four mechanisms are thermally driven channeling, downward momentum transport, forced channeling, and pressure-driven channeling. Each physical mechanism possesses a unique signature in plots of the joint frequency distributions of the above-valley wind directions versus valley wind directions. These idealized signatures, adapted after Whiteman

* Current affiliation: Science and Technology Branch, Environment Canada, Toronto, Ontario, Canada.

*Corresponding author address:* Dr. Marco L. Carrera, Environment Canada, Meteorological Research Division, Canadian Meteorological Centre, 5th Floor, 2121 Trans-Canada Highway, Dorval, QC H9P 1J3, Canada.
E-mail: marco.carrera@ec.gc.ca

DOI: 10.1175/2009JAMC2061.1

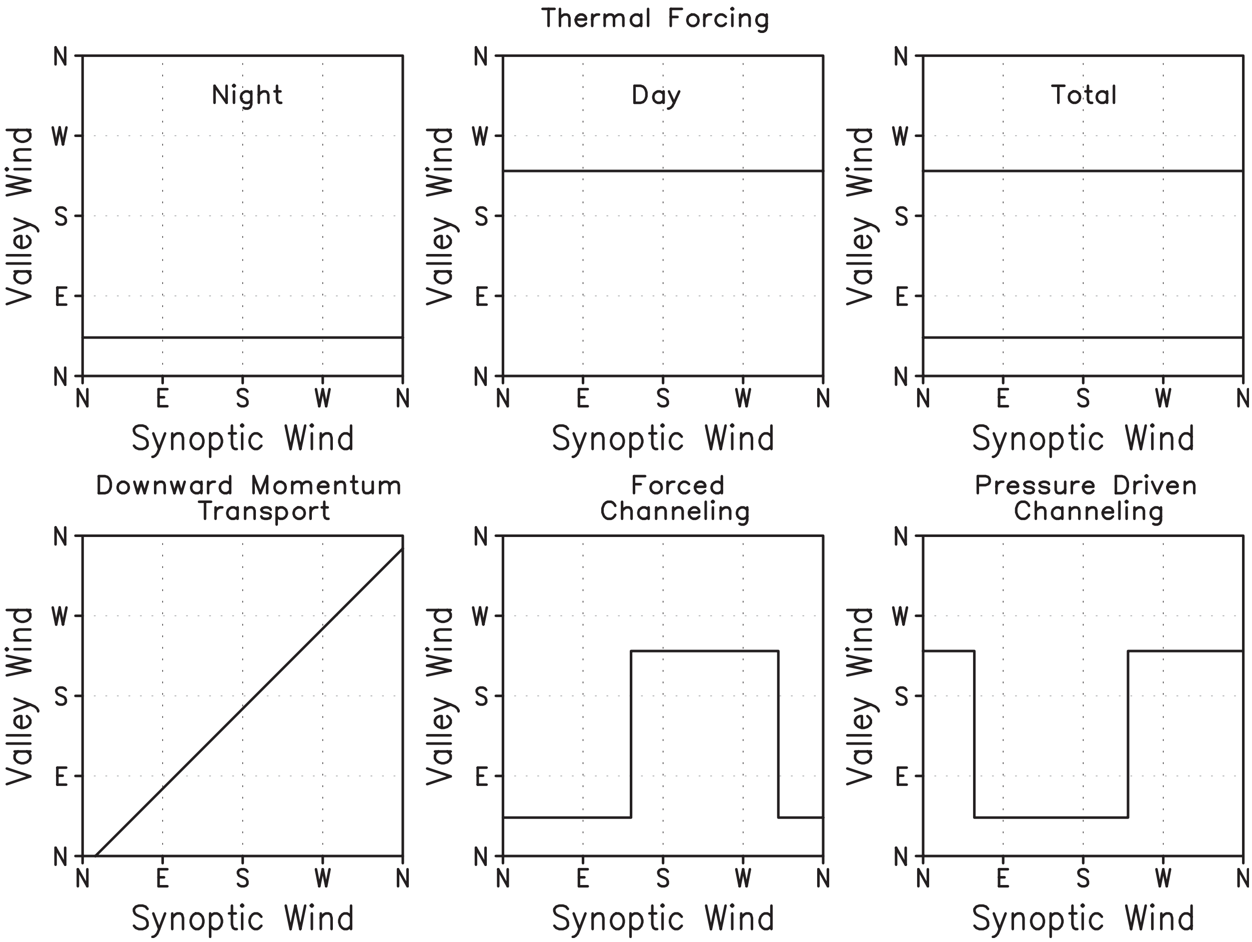


FIG. 1. Relationships between synoptic (above-valley geostrophic) and valley wind directions for four possible forcing mechanisms: thermal forcing, downward momentum transport, forced channeling, and pressure-driven channeling. The valley is assumed to be oriented from northeast to southwest. Adapted from Whiteman and Doran (1993).

and Doran (1993), are shown in Fig. 1. The wind climatology of a given valley is often the result of varying contributions from these four mechanisms.

For the thermal forcing mechanism, winds within the valley respond to the along-valley pressure gradients that develop as a hydrostatic response to temperature differences that form along the valley axis. The within-valley winds do not depend upon the geostrophic wind direction above the valley. As expected there is a diurnal reversal in wind directions, with generally up-valley winds during the daytime and down-valley winds during the nighttime (Fig. 1). Note that for the assumed northeast–southwest-oriented valley in Fig. 1, the southwest winds shown during the daytime and the northeast winds during the nighttime are strictly valid if the valley widens to a degree where it can be considered a plain at the southwest end (Rampanelli et al. 2004). Local wind systems that are thermally induced are favored when geostrophic winds above the valley are weak (Stewart et al. 2002).

When downward momentum transport is the dominant mechanism, the valley wind directions are similar to the above valley geostrophic wind directions with a slight turning (~25°) toward lower pressure with decreasing height (Fig. 1). This mechanism is most likely to occur in unstable or neutrally stratified atmospheric conditions when there is stronger coupling between the valley winds and the above-valley geostrophic winds. The configuration of the valley also plays a role, with wide flat-bottomed valleys and low sidewalls favoring the downward transport of momentum (Whiteman and Doran 1993).

The third process is termed forced channeling and occurs when the winds above the valley are in geostrophic balance, but as the ground is approached, the winds are forced to flow along the valley axis (Fig. 1). The valley wind direction and speed are functions of the sign and magnitude of the above valley wind projected along the valley axis. A unique feature of this mechanism is the 180° shift in valley wind direction when the geostrophic or above-valley wind crosses an axis perpendicular to the valley (Weber and Kaufmann 1998). Forced channeling mechanisms are expected to be important for narrow valleys during unstable or neutral conditions (Whiteman and Doran 1993; Weber and Kaufmann 1998).

The final mechanism is pressure-driven channeling in which the valley winds are driven by the component of the pressure gradient along the valley axis. Unlike the forced channeling mechanism, the valley winds shift direction by 180° when the geostrophic or above-valley wind crosses an axis that runs along the valley (Fig. 1). Pressure-driven channeling has been shown to be prominent in wide and shallow valleys under light–moderately stable atmospheric conditions (Gross and Wippermann 1987; Whiteman and Doran 1993; Weber and Kaufmann 1998; Kossmann and Sturman 2003). A unique feature of pressure-driven channeling is the presence of countercurrents. Countercurrents occur when the velocity component of the wind within the valley is opposite to the component above the valley. Gross and Wippermann (1987) documented the existence of countercurrents in association with pressure-driven channeling in the upper Rhine Valley, while Whiteman and Doran (1993) did the same for the Tennessee Valley in the United States.

Gap winds or gap flows refer to airflow between indentations in mountain ranges, which may result from purely horizontal constrictions (level gaps) or constrictions that are both horizontal and vertical such as mountain passes (Mayr et al. 2004, 2007). These gap winds occur in the presence of a pressure gradient that exists in the along-gap direction (Lackmann and Overland 1989; Colle and Mass 1998; Steenburgh et al. 1998; Mayr et al. 2004; Gaberšek and Durran 2006; Mayr et al. 2007). Several studies have documented gap winds that are primarily driven by the large-scale pressure gradient, including gap winds in the Shelikof Strait of Alaska (Lackmann and Overland 1989), the Cook Strait separating the North and South Islands of New Zealand (Reid 1996), the Columbia Gorge in the northwestern United States (Sharp and Mass 2002), and the Petaluma Pass in northern California (Neiman et al. 2006). As Colle and Mass (1998) point out, a series of theoretical and observational studies in the 1980s and early to mid-1990s supported a conceptual model for the ageostrophic along-gap wind in which there is a three-way balance between acceleration, the pressure gradient force, and surface friction (Overland 1984).

More recent studies, both observation and model based, of gap flows along the west coast of North America and the Alps in Europe point to the increasing importance of mesoscale circulations in enhancing the strength of gap winds (Colle and Mass 1998, 2000; Mayr et al. 2004, 2007). Mayr et al. (2007) provide a thorough review of the increased understanding of gap flows garnered through the Mesoscale Alpine Programme (MAP) experiment. These studies benefitted from high spatial and temporal resolution observation networks to accurately document the three-dimensional structures of gap flows including the upstream and downstream reservoirs (Mayr et al. 2007). Gaberšek and Durran (2006) in their idealized study of long gap flows found that mesoscale pressure perturbations associated with mountain waves and upstream blocking can create pressure gradients along the gap that are different from the synoptic scale and can act to reinforce the strength of the gap winds.

The St. Lawrence River Valley (SLRV) is a primary topographic feature of eastern Canada, extending in a southwest–northeast direction from Lake Ontario, past Montreal (YUL) and Quebec City (YQB), and terminating in the Gulf of St. Lawrence (see Fig. 2a). It has long been known to forecasters in eastern Canada that, under certain preferred distributions of the synoptic-scale pressure field and atmospheric stability, the winds within the SLRV can become channeled in the direction of the component of the pressure gradient force aligned along the valley axis (Powe 1968; Cohn et al. 1996; Slonosky 2003; Roebber and Gyakum 2003)—so-called pressure-driven channeling. Evidence of the pronounced wind channeling at Quebec City dates back to the earliest known instrumental meteorological observations for Canada, those taken by the French physician Dr. Jean-Francois Gaultier (Slonosky 2003). His observations for the period 1742–56 indicated that the most prominent wind directions at Quebec City were from the southwest and northeast (Slonosky 2003).

Although the width of the St. Lawrence River in the vicinity of Quebec City is narrow (~3 km), the width of the SLRV is on the order of 50 km (Fig. 2b). To the north the Laurentian Mountains are steeply sloped, while the valley is gently sloping for a considerable distance to the south (Fig. 2b). To the southwest of Quebec City the SLRV broadens considerably (Fig. 2b). Closer to Montreal the SLRV is noticeably flat, possessing a width of roughly 90 km (Fig. 2b). To the south of Montreal lies the Lake Champlain Valley (LCV), situated on the border of New York State and Vermont, which leads to the Hudson River Valley (Fig. 2a). The Adirondack Mountains are located to the west in New York, while to the east lie the Green Mountains of Vermont. The width of the LCV in the vicinity of Burlington, Vermont (BTV), is roughly 30 km and the valley extends a considerable distance southward, of particular importance

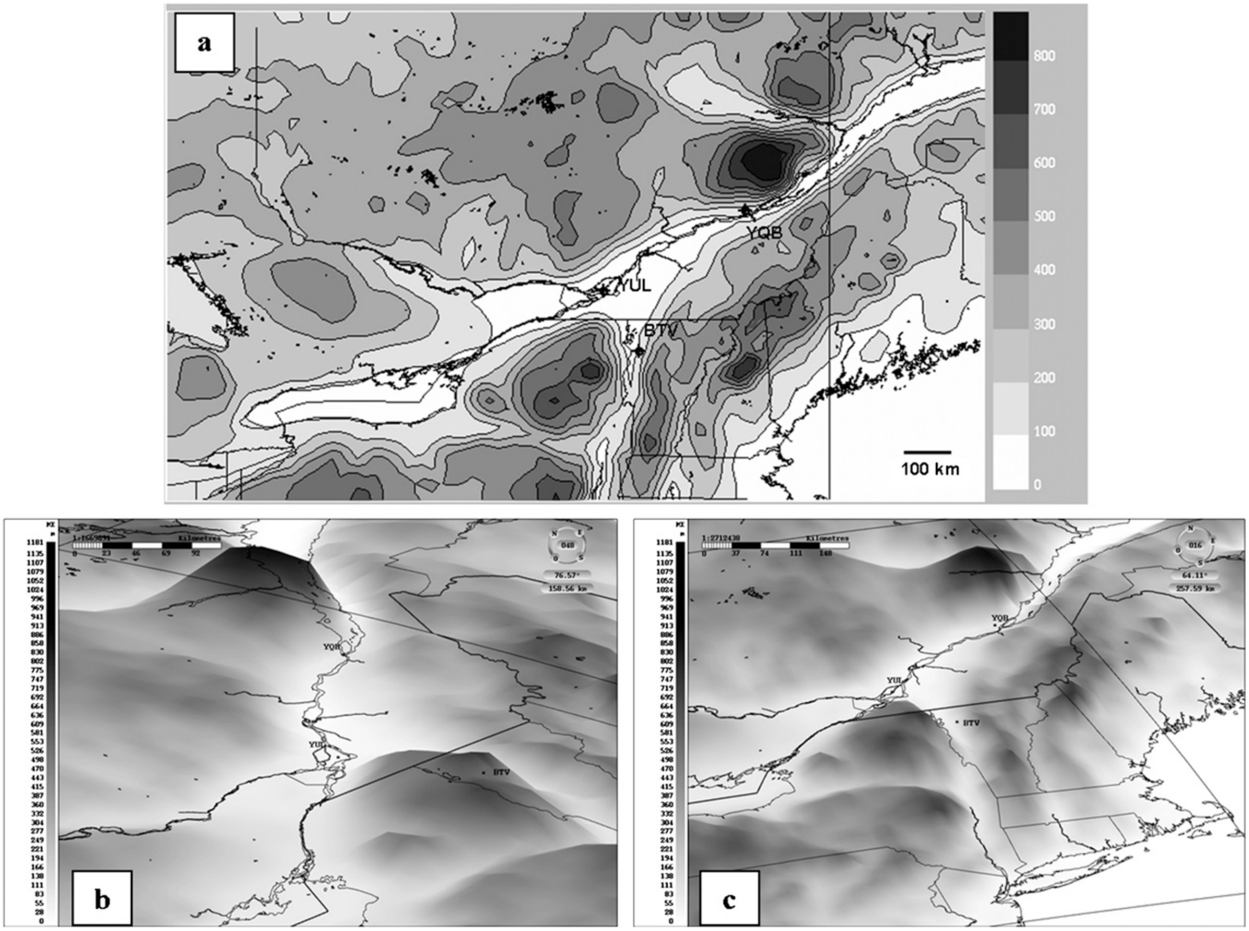


FIG. 2. (a) Topographic map (m) of SLRV and LCV regions. The topographic information was obtained from a U.S. Geological Survey (USGS) global 1-km database. The locations of the three meteorological stations used in this study—YUL, YQB, and BTV—are shown. 3D perspectives of the SLRV and LCV regions as seen from the (b) southwest and (c) south.

for southerly winds (Fig. 2c). Lake Champlain lies within the LCV, possessing a surface area of 1127 km$^2$, which is considerably smaller than that of the Great Lakes. However, the lake itself is over 190 km in length with a maximum width of 19 km and exerts an important influence on the local weather (Payer et al. 2007; Laird et al. 2009).

Surface wind channeling is very common in the north–south-oriented LCV, and National Weather Service (NWS) forecasters are aware of the potential hazards that the enhanced low-level winds pose to marine and aviation interests in the valley (J. Goff, NWS, 2008, personal communication). Laird et al. (2009) examined events of lake-effect precipitation over Lake Champlain for the 9-yr period 1997/98 through 2005/06 and found that the dominant wind direction for lake-effect snowfall events was along the major axis of Lake Champlain. Close to 25% of the isolated Lake Champlain lake-effect precipitation bands were found to occur during periods of southerly winds (Laird et al. 2009).

Roebber and Gyakum (2003) undertook a detailed mesoscale analysis of the extreme ice storm of 1998 over the eastern Canadian provinces and the northeastern United States. In particular, the authors demonstrated that the position of the surface-based freezing line was strongly linked to the orographic channeling of the cold air within the SLRV. Additionally, the presence of low-level geostrophic southerly (warm) winds throughout the period acted to create an intense surface-based temperature inversion. Subfreezing air extended upward to nearly 850 hPa, with a 10°C rise in temperature between 950 and 800 hPa (Roebber and Gyakum 2003). The presence of northeasterly surface winds combined with southerly geostrophic winds is indicative of countercurrents and acted to create conditions conducive to the formation of freezing precipitation (Cortinas 2000). The orographic channeling of the cold air was also shown to be important in providing a frontogenetic focus along the United States–Canada border (Roebber and Gyakum 2003). Model sensitivity tests performed indicated that in the absence of orographic channeling, little or no freezing precipitation would have occurred at Burlington (Roebber and Gyakum 2003).

Roebber and Gyakum (2003) argue that large-scale factors combined with the orographic forcing provide a mesoscale focus for the frequent occurrence of freezing rain for the SLRV. Indeed the studies of Laflamme and Périard (1998), Stuart and Isaac (1999), Cortinas (2000), and Cortinas et al. (2004) support the notion of the SLRV as a local maximum in the annual occurrence of freezing rain days. Stuart and Isaac (1999), in their study of freezing rain over Canada, examined the dominant wind directions during freezing rain events at Montreal and found that these events were strongly correlated with northeasterly surface winds, suggesting an important channeling effect associated with the orientation of the SLRV. Predictability of these events of pressure-driven channeling at the mesoscale requires accurate prediction at synoptic and larger scales.

Owing to the important linkage between wind channeling within the SLRV and the occurrence of freezing precipitation, the objective of this study is to examine the long-term surface wind climatology within the SLRV and the LCV. In particular, we will investigate the importance of the large-scale or synoptic controls upon the surface wind channeling within the SLRV and the LCV and within the context of the classical dynamical mechanisms described in Whiteman and Doran (1993). These classical mechanisms are particularly well suited for this task and have been used to study wind channeling in several valleys around the world (Gross and Wippermann 1987; Weber and Kaufmann 1998; Eckman 1998; Nawri and Stewart 2006, 2008; Zhong et al. 2008). The pressure-driven channeling, documented by Roebber and Gyakum (2003) as fundamental to the longevity and severity of the 1998 ice storm, will be put into a climatological context. Similar to the study of the wind climatology for the upper Rhine Valley (Gross and Wippermann 1987), we will document the existence of countercurrents associated with pressure-driven channeling of the surface winds within the SLRV.

The outline of the paper is as follows: in section 2 we discuss the datasets used in this study. The surface- and ridge-level wind climatologies at Montreal, Quebec City, and Burlington are discussed in section 3. In section 4 we document the relationship between the ridge-level and valley winds by examining the importance of the four physical mechanisms discussed above. Discussion is provided in section 5 and conclusions are given in section 6.

## 2. Data and methodology

There are two principal sources of data utilized in this study. To document the hourly surface winds within the SLRV and LCV we utilize three representative meteorological stations whose locations are shown in Fig. 2a. For the SLRV, Pierre Elliott Trudeau International Airport located in Dorval, Canada, and Jean Lesage International Airport in Quebec City possess hourly measurements of surface winds that date back to the early 1950s. Prior to 1972 wind directions were recorded with a directional precision of 16 possible directions, while after 1971 directions were recorded with a precision of 10° resulting in 36 possible directions. These data are available in the digital archive of Canadian climatological data from Environment Canada. Hourly surface winds at Burlington located on the eastern shores of Lake Champlain are used to characterize the surface winds within the LCV. The data for BTV were obtained from the National Climatic Data Center (NCDC) surface hourly data archive. Similar to the Canadian stations after 1971, the wind directions at Burlington are recorded with a directional precision of 10°. The elevations of the respective stations are 31 m (YUL), 70 m (YQB), and 101 m (BTV). At all three stations wind measurements are taken at the standard 10 m above ground level.

The recently released North American Regional Reanalysis (NARR) dataset (Mesinger et al. 2006) is used to characterize the geostrophic winds above ridge height and to analyze the sea level pressure (SLP) and lower-tropospheric temperature structures during channeling events. The NARR is a long-term, high-resolution dataset for the study of climate- and hydrological-related phenomenon, extending over the period 1979–2002 and is continued in near–real time as the Regional Climate Data Assimilation System (RCDAS). The essential components of the NARR are the National Centers for Environmental Prediction (NCEP) Eta Model and its Data Assimilation System (EDAS) and the Noah land surface model (Mesinger et al. 2006). The Eta Model used for the production of the NARR has a 32-km horizontal resolution with 45 layers in the vertical, with analyses performed every 3 h. For more details on the NARR please refer to Mesinger et al. (2006).

Our analysis period starts in 1979 to coincide with the start time of the NARR. A problem was discovered with the precipitation assimilation in the RCDAS system, which affects the period January 2003–December 2004. At the time of this writing, scientists at NCEP are currently rerunning the RCDAS system to correct this problem. For this reason we end our analysis in December 2002 and consider the 24-yr period 1979–2002 as our study period.

## 3. Surface and ridge-level wind climatologies for YUL, YQB, and BTV

In this section we document the long-term surface wind and ridge-level wind climatologies for YUL, YQB, and BTV as a function of season. Seasons are defined as winter [December–February (DJF)], spring [March–May (MAM)], summer [June–August (JJA)], and fall [September–November (SON)].

### *a. Surface wind climatology*

In Figs. 3, 4, and 5 we show wind rose diagrams, which depict the mean wind speed by directional sectors, for YUL, YQB, and BTV as a function of season for the 24-yr period 1979–2002. For clarity we have chosen to show only 16 wind direction sectors at each station. On each wind rose, concentric frequency circles are drawn at intervals of 5%, with the mean wind speed for each directional petal shown.

At Montreal the surface winds are predominantly west-southwesterly throughout the year (Fig. 3). The occurrence of northeasterly surface winds is most pronounced during the winter (Fig. 3a) and spring (Fig. 3b) seasons. If we refer back to Fig. 2 we note that the bidirectionality in the surface wind distribution (i.e., westerly-southwesterly and northeasterly) is consistent with the orientation of the SLRV in the vicinity of Montreal. It is interesting to note the more frequent occurrence of southeasterly surface winds in the spring (Fig. 3b) and fall seasons (Fig. 3d), which is most likely related to outflow from the LCV (see Fig. 2). The average wind speeds for the directional sectors indicate that the mean wind speeds are generally highest for the west-southwesterly and northeasterly directions.

The wind rose diagrams for Quebec City are plotted in Fig. 4. A clear bidirectionality in the surface wind directions is evident throughout all seasons. The channeling efficiency is more pronounced at YQB, when compared with YUL, as surface winds are either west-southwesterly or east-northeasterly over 50% of the time. Referring back to Fig. 2, the enhanced channeling at YQB is supported by the consistent orientation of the terrain of the SLRV over a greater distance. Note that the orientation of the SLRV at YQB is different than at YUL, shifted to a more west-southwest/east-northeast direction (see Fig. 2b). The occurrence of east-northeasterly winds is a maximum in the spring season (Fig. 4b).

Wind rose diagrams for Burlington are shown in Fig. 5. A bidirectionality in surface wind directions, northerly and southerly, is clearly present. The most prominent wind direction is southerly, consistent throughout the year ($\sim$22% of the time). Winds from the north and northwest sectors are present throughout all seasons, but are most prominent during the spring period (Fig. 5b). Southwesterly surface winds at BTV are not very common.

### *b. 925-hPa geostrophic wind climatology*

To investigate the channeling effect of the SLRV we need to estimate the ambient winds above the valley. In the following discussion the term ambient winds implies the geostrophic winds above ridge height. We use the 925-hPa geostrophic winds to represent winds above the valley. The 925-hPa level is typically found at an elevation of roughly 700 m above mean sea level (MSL), which is higher than any of the valley walls of the SLRV and the LCV (see Fig. 2) and thus unlikely to be influenced by channeling effects within either valley. One approach to estimate the geostrophic winds at 925 hPa is to utilize a weighted average of the geostrophic winds derived from the closest upper-air rawinsonde stations (e.g., Whiteman and Doran 1993; Weber and Kaufmann 1998). As discussed by Eckman (1998) this method has an advantage because actual observed rawinsonde data are used. The major disadvantage is that rawinsonde observations are available only twice daily, at 0000 and 1200 UTC, which limits the sample size to compare with the hourly surface wind observations. Furthermore, these observing times (i.e., 0000 and 1200 UTC) are often close to sunrise and sunset where the boundary layer undergoes periods of transition, further complicating physical interpretations (Eckman 1998).

In this study, we calculate the 925-hPa geostrophic winds from the recently released NARR (Mesinger et al. 2006). The original NARR dataset is available on the Advanced Weather Interactive Processing System (AWIPS) 221 grid, which has a Lambert conformal projection with a horizontal resolution of approximately 32 km. This grid projection is difficult to work with (i.e., calculation of derivatives) and so the data were interpolated onto a regular $0.5° \times 0.5°$ latitude–longitude grid. Taking the nearest grid point to each station, YUL, YQB, and BTV, we calculated the zonal and meridional components of the 925-hPa geopotential height gradient using a finite-difference scheme. From these gradient calculations we then calculated the zonal and meridional components of the 925-hPa geostrophic wind at each station. The result is a 925-hPa geostrophic wind dataset at 3-hourly resolution for YUL, YQB, and BTV for the period 1979–2002.

Mesinger et al. (2006) undertook a detailed comparison of the NARR surface and upper-air data with both observations and the NCEP–Department of Energy (DOE) global reanalysis. Results from comparisons of rawinsonde temperature and wind data indicate that the NARR represents a considerable improvement over the

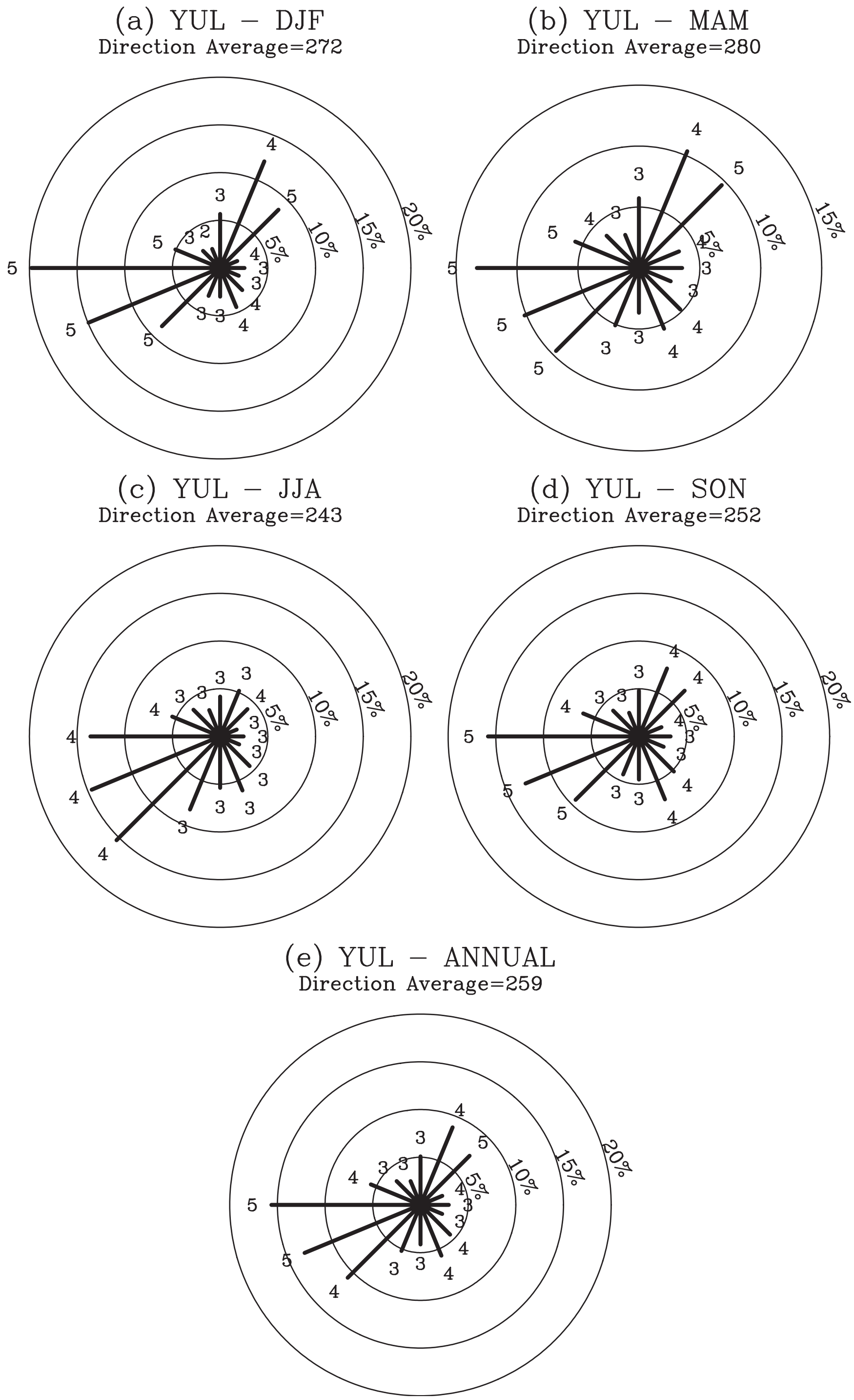


FIG. 3. Surface wind rose diagrams for YUL as a function of season for the period 1979–2002: (a) DJF, (b) MAM, (c) JJA, (d) SON, and (e) annual. Concentric frequency rings are plotted at intervals of 5%, with the mean wind speed (m $s^{-1}$) indicated at the end of each directional petal of the wind rose.

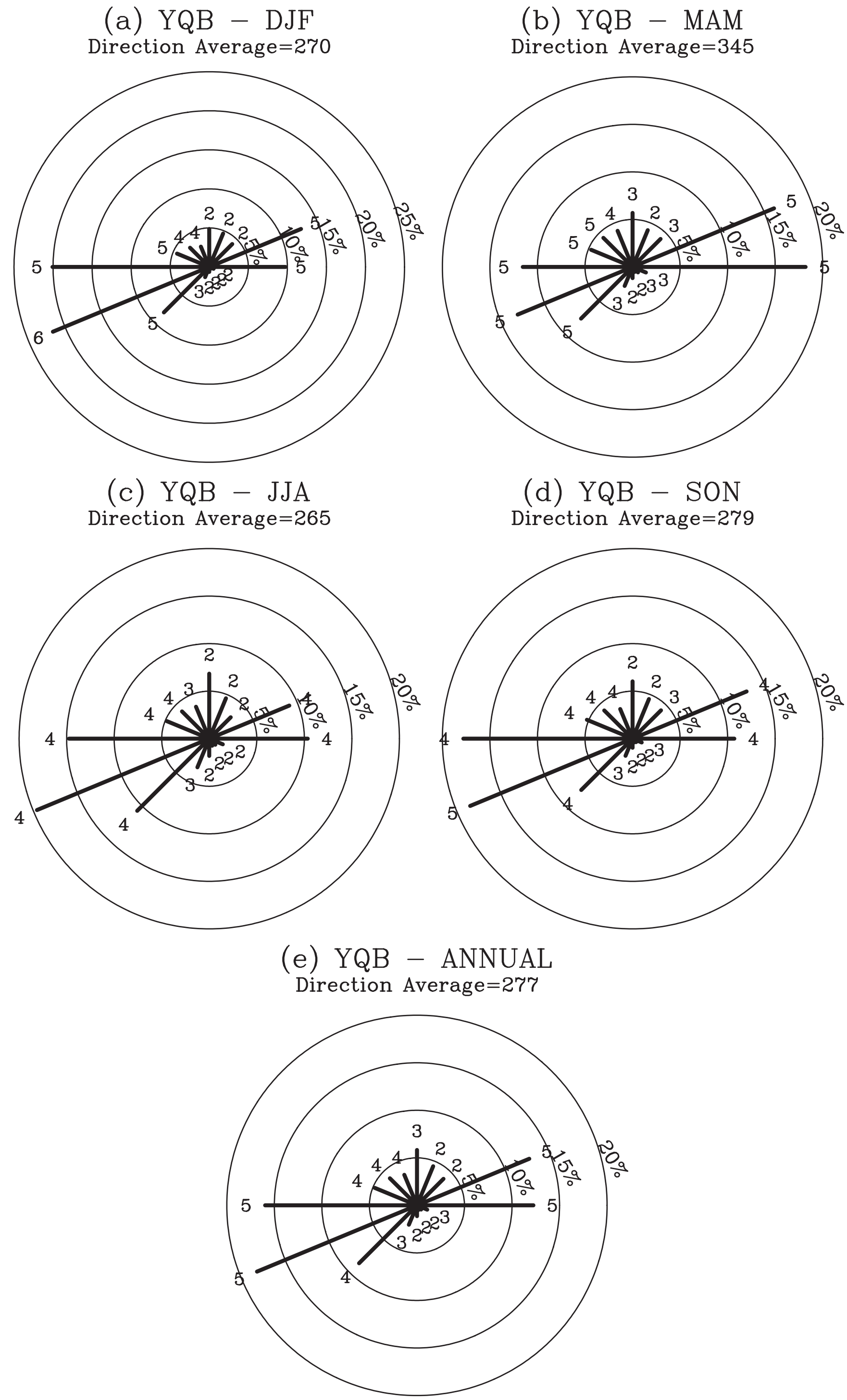


FIG. 4. As in Fig. 3, but for YQB.

NCEP–DOE global reanalysis (Mesinger et al. 2006). This improvement not only applies to the NARR, but also to the more independent comparison of the respective first-guess fields from the NARR and NCEP–DOE fields. Zhong et al. (2008) in their study of high-wind events in Owens Valley, California, made use of the NARR upper-level wind data to characterize synoptic-scale winds above the valley.

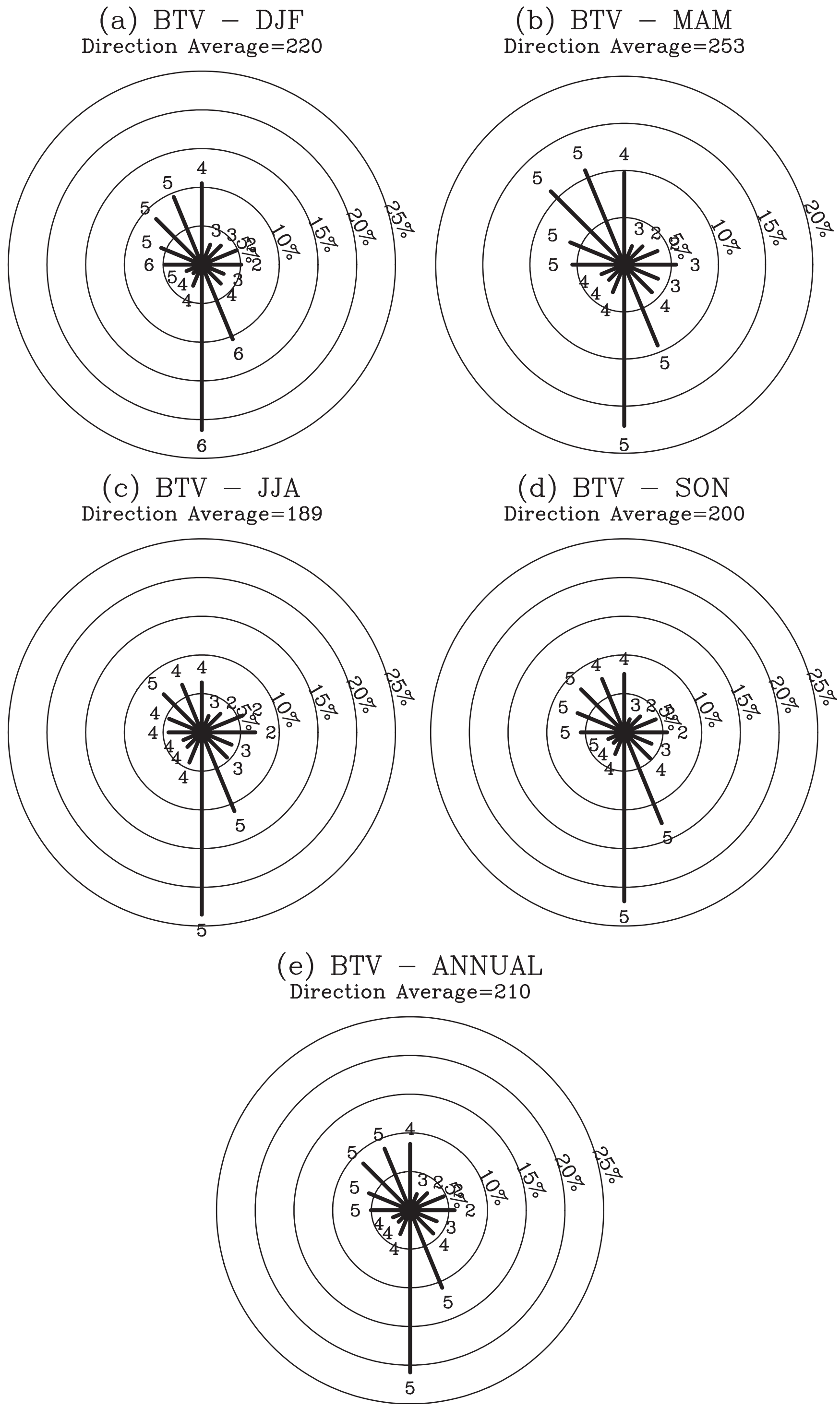


FIG. 5. As in Fig. 4, but for BTV.

Wind rose diagrams for the 925-hPa geostrophic winds for YUL and YQB are shown in Figs. 6 and 7, respectively. At both locations the prevailing geostrophic winds at 925 hPa are predominantly westerly throughout all seasons. As is to be expected, the mean wind speeds are greatest (smallest) during the winter (summer) season for both locations. At YQB (Fig. 6) the 925-hPa geostrophic winds have a more pronounced

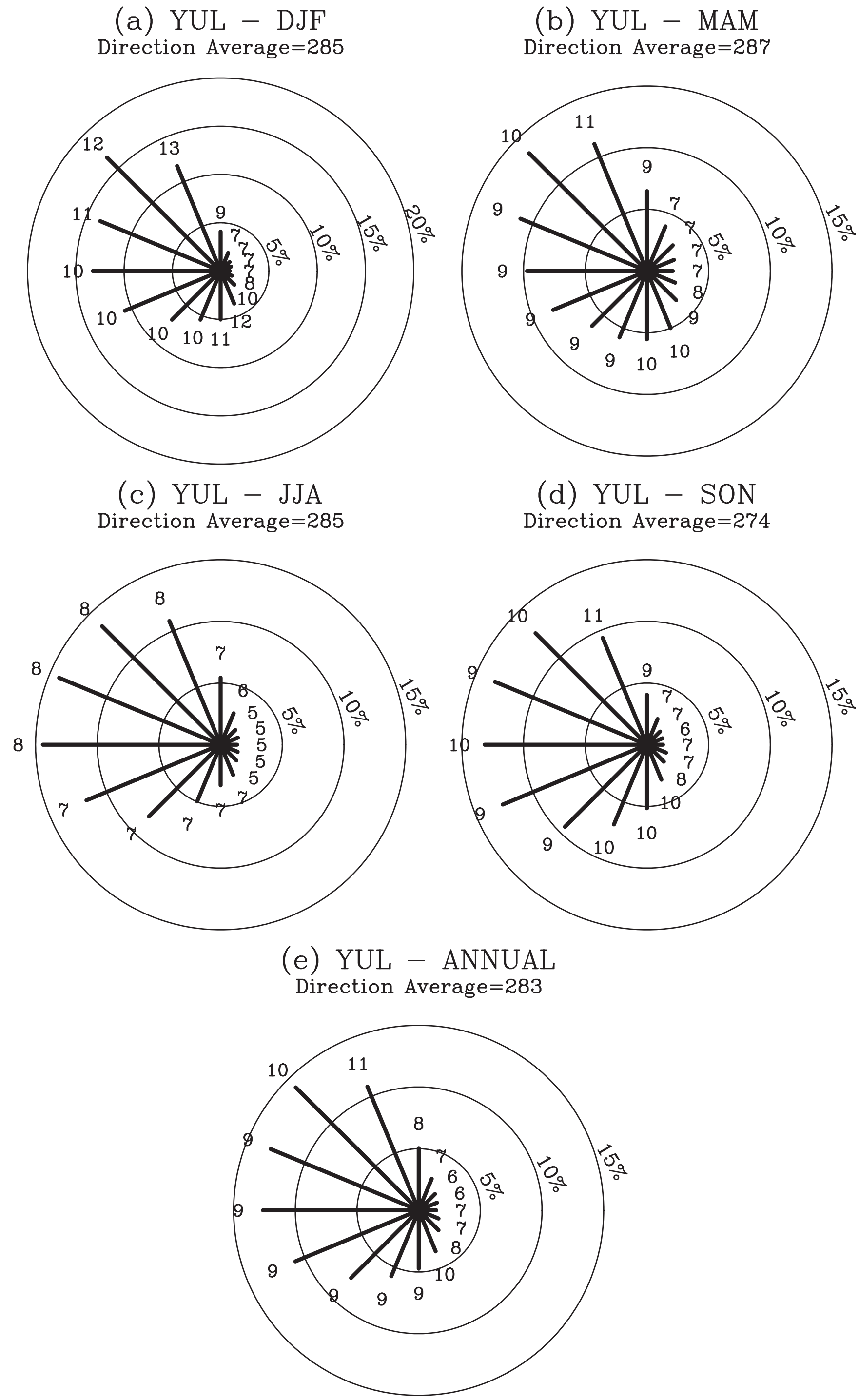


FIG. 6. Wind rose diagrams for the geostrophic wind at 925 hPa as a function of season for the period 1979–2002 for YUL: (a) DJF, (b) MAM, (c) JJA, (d) SON, and (e) annual. Concentric frequency rings are plotted at intervals of 5%, with the mean wind speed (m $s^{-1}$) indicated at the end of each directional petal of the wind rose.

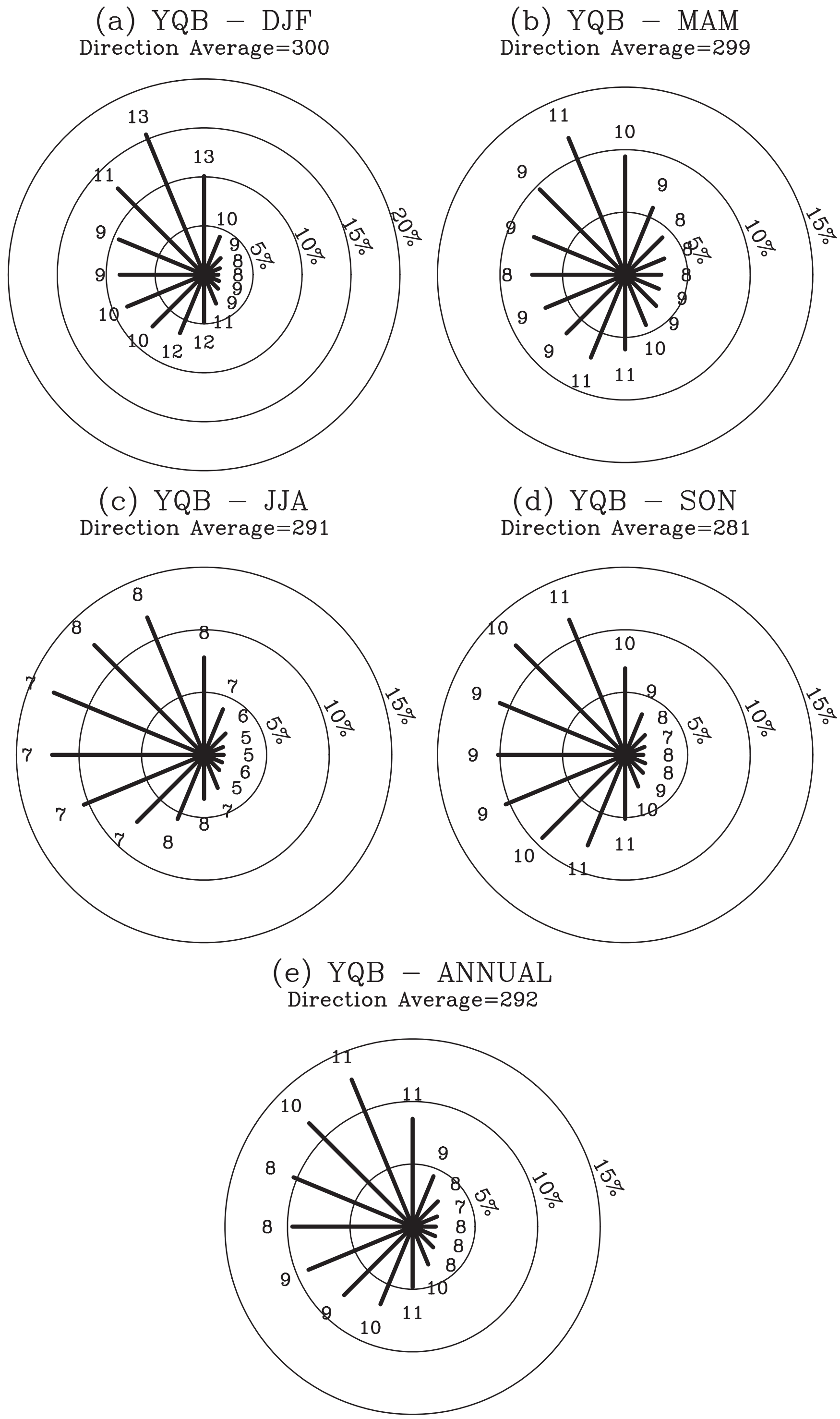


FIG. 7. As in Fig. 6, but for YQB.

northwesterly component, when compared with YUL (Fig. 6). The wind roses at 925 hPa for both YUL and YQB are much broader and are not bidirectional as was seen for the surface wind roses (Figs. 3, 4) indicating that the 925-hPa level is at a high enough altitude to not be influenced by the valley channeling effects. We have not shown the wind roses for the 925-hPa geostrophic winds at BTV as they are very similar to both YUL and YQB,

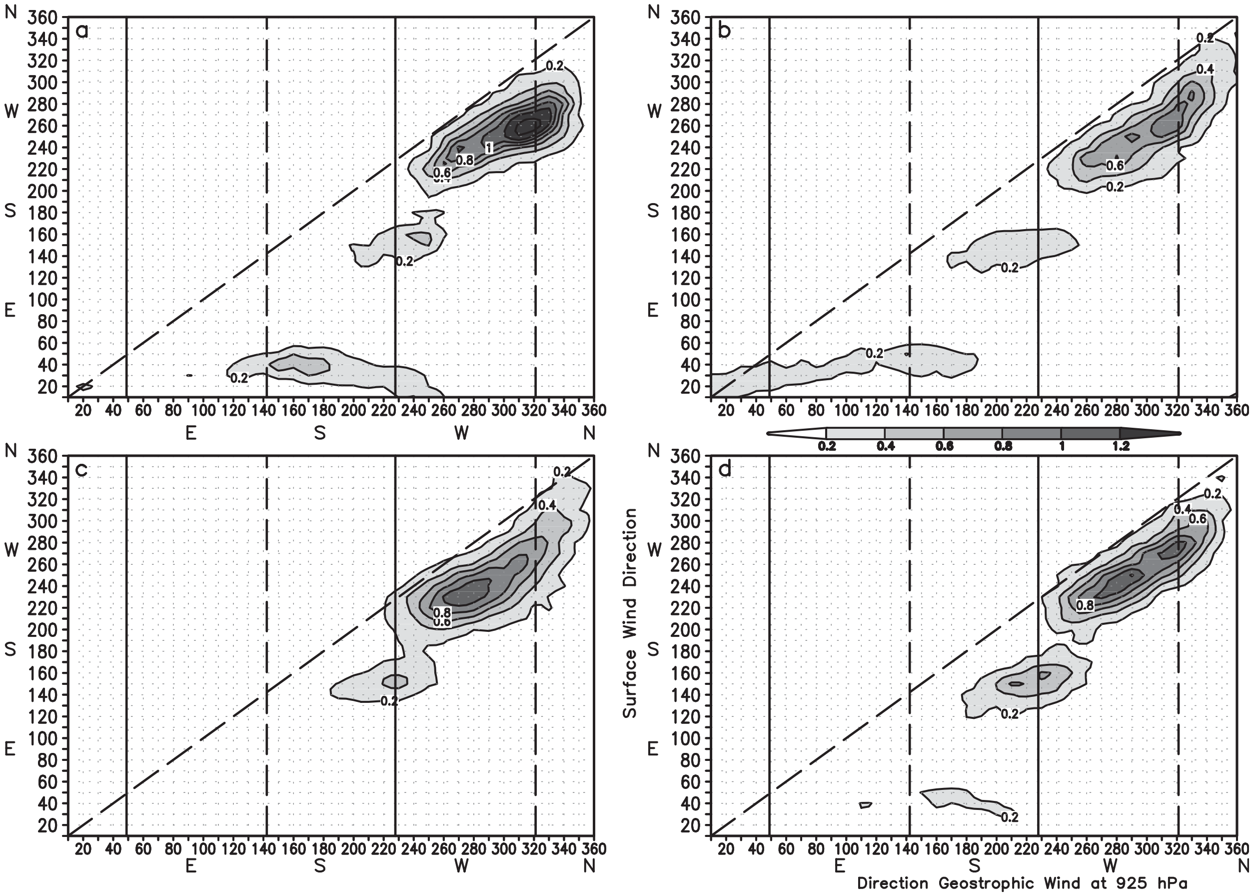


FIG. 8. Joint frequency distributions of surface wind directions (ordinate) vs 925-hPa geostrophic wind directions (abscissa) for YUL for the period 1979–2002: (a) DJF, (b) MAM, (c) JJA, and (d) SON. Solid (dashed) lines represent axes that are parallel (normal) to the mean axis of the SLRV. The diagonal dashed line represents a line for which the 925-hPa geostrophic wind direction is the same as the valley wind direction.

except for an increase in the southwesterly geostrophic wind frequency (see Fig. 10).

## 4. Relationship between ambient and valley winds

In this section we investigate the relationships between the above-valley winds and the winds within the valley for both the SLRV and the LCV. In Figs. 8, 9, and 10 we show plots of the joint frequency distribution of the ambient wind directions, as represented by the 925-hPa geostrophic winds, and the valley wind directions for YUL, YQB, and BTV as a function of season. Examining the joint frequency distributions facilitates the task of identifying the physical mechanism(s) responsible for the observed ambient wind–valley wind relationships, as each physical mechanism has a unique signature (see Fig. 1). As discussed in the introduction, the four different physical mechanisms are associated with distinct conceptual joint frequency distributions of the ambient wind and valley wind directions. Often the situation is such that different forcing mechanisms can be superimposed at the same location with the relative importance being a function of the geostrophic wind speed.

### *a. Montreal*

Examining the joint frequency distributions for YUL (Fig. 8), we can identify downward momentum transport as being a prominent mechanism for geostrophic wind directions ranging from 240° to 340° (i.e., southwesterly to northwesterly). The surface wind directions follow those of the 925-hPa geostrophic wind with a characteristic turning of roughly 25°–30° toward lower pressure with decreasing elevation. This downward momentum transport appears to be most pronounced during the DJF period and increases in importance as the strength of the 925-hPa geostrophic winds increases (not shown). During the JJA period, for surface wind directions ranging from 240° to 300° there is an increased spread in the associated 925-hPa geostrophic wind directions for a

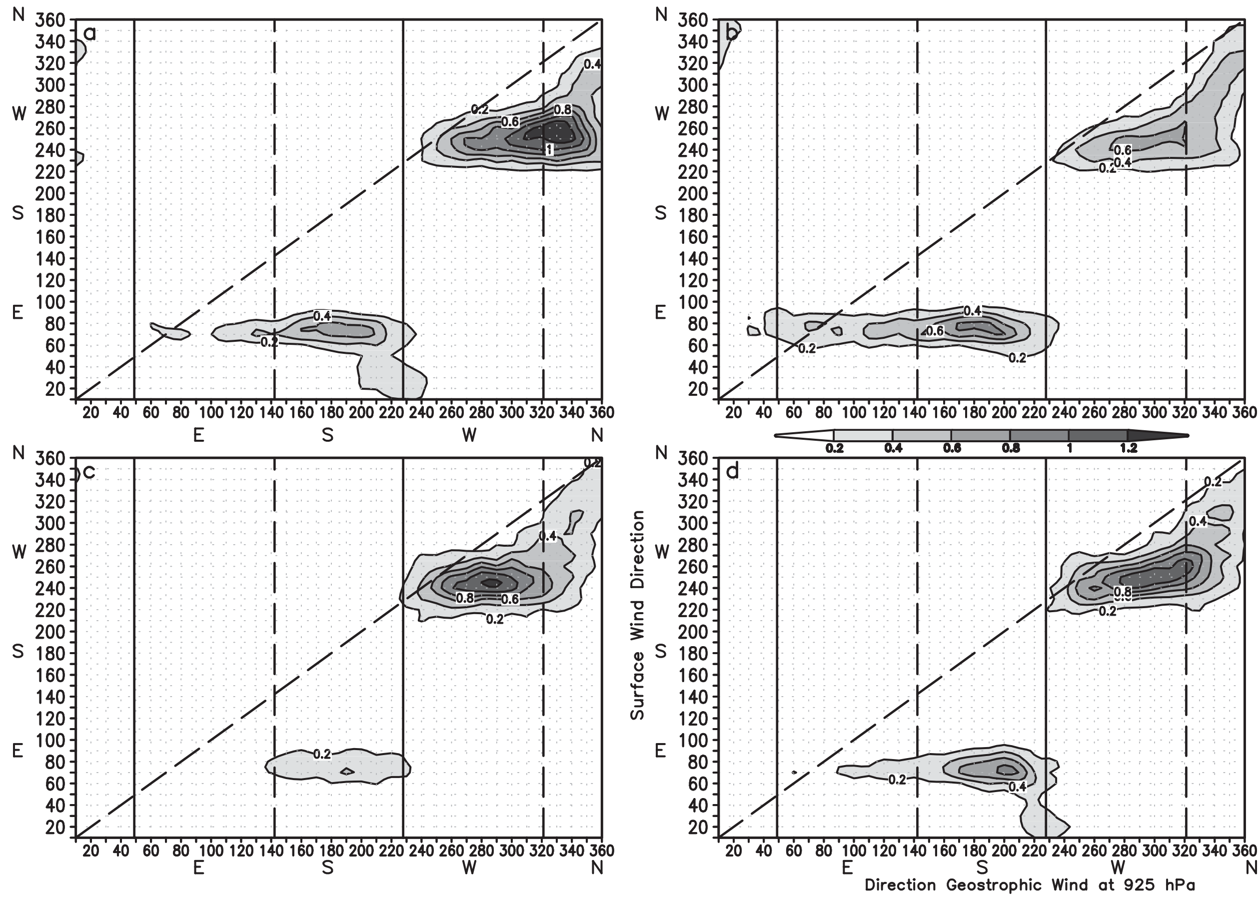


FIG. 9. As in Fig. 8, but for YQB.

given surface wind direction (Fig. 8c), implying a reduced importance of downward momentum transport.

A series of four vertical lines are plotted in Figs. 8a–d. The solid (dashed) lines represent axes that are parallel (normal) to the mean axis of the SLRV at YUL. If we examine more closely the solid lines that are parallel to the axis of the SLRV, especially the line centered at roughly 230°, we note a distinct signature of pressure-driven channeling during the winter, spring, and fall periods (Figs. 8a,b,d). Recall that for the pressure-driven channeling mechanism we witness a shift in surface wind direction of 180° when the geostrophic or above-valley wind direction crosses an axis that runs along the valley. For the DJF period (Fig. 8a) the sudden shift in surface wind directions from roughly 30° (northeasterly) to 220° (southwesterly) is clearly evident as the geostrophic wind directions at 925 hPa shift across the 230° axis. For a small change in the 925-hPa geostrophic wind direction around 230°, several different surface wind directions are possible.

A secondary southeasterly surface wind maximum, centered at roughly 150°, is present to varying degrees in all seasons (Figs. 3, 8). The joint frequency distribution plots in Fig. 8 indicate that the occurrence of these southeasterly surface winds at YUL is associated with 925-hPa geostrophic wind directions between 180° (southerly) and 260° (west-southweasterly), centered near 230°. These surface winds are not aligned along the mean axis of the SLRV. We suggest that these southeasterly surface winds represent outflow from the LCV to the southeast. We will come back to this point later in the discussion section.

The local maximum in the joint frequency distribution during DJF, which is centered between surface wind directions 20° and 50° (Fig. 8a), is of particular interest. These surface wind directions represent northeasterly flow along the axis of the SLRV (see Fig. 2). The associated 925-hPa geostrophic winds are concentrated between 120° and 240° with a local maximum near 170°. This area on the joint frequency distribution represents countercurrents, whereby the velocity component of the wind projected within the valley (northeasterly) is opposite to the above-valley wind component projected within the valley, which is southwesterly. We note that

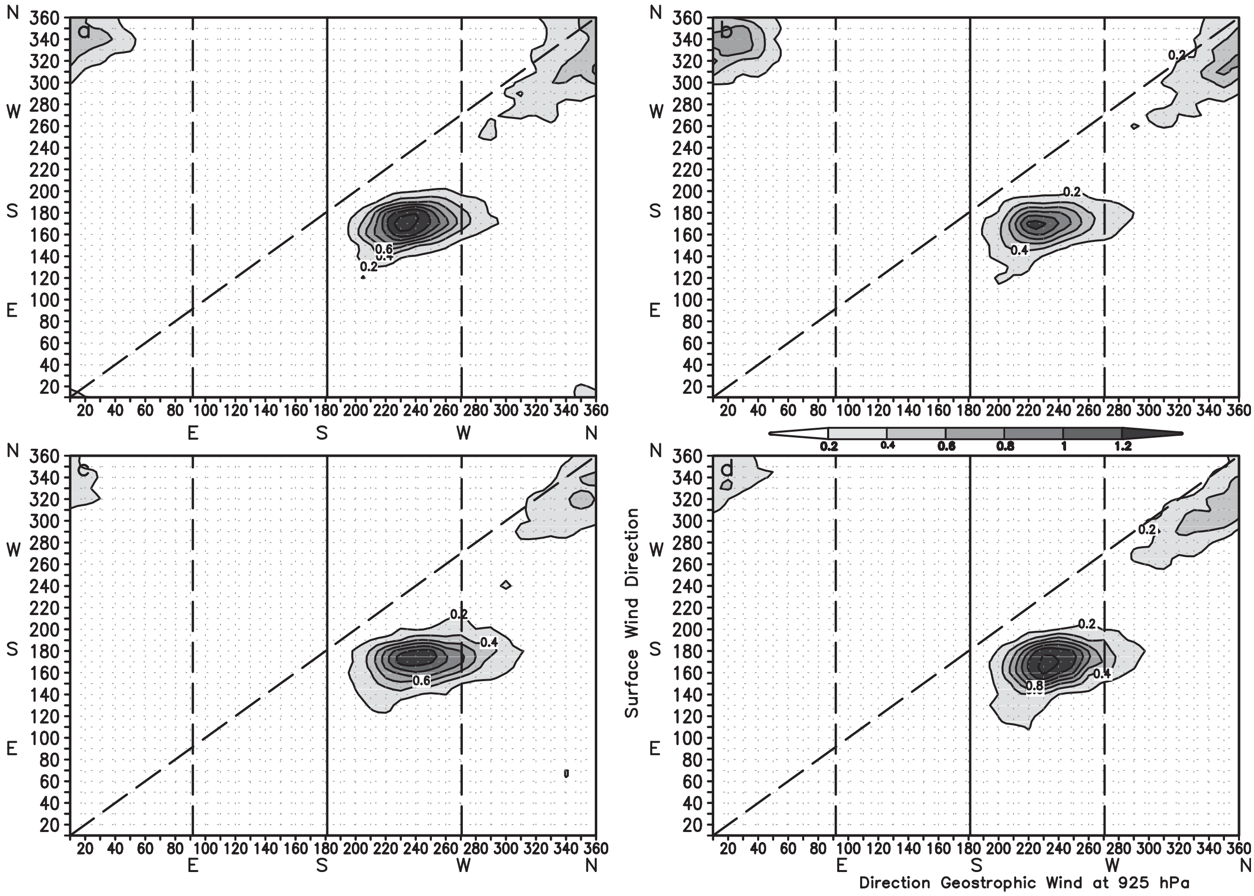


FIG. 10. As in Fig. 8, but for BTV. Solid (dashed) lines represent axes that are parallel (normal) to the mean axis of the LCV.

countercurrents for surface northeasterlies are also present in the spring (Fig. 8b) and fall (Fig. 8d) seasons, but are absent during the summer (Fig. 8c). Gross and Wippermann (1987) demonstrated that countercurrents in the upper Rhine Valley were often associated with pressure-driven channeling.

## *b. Quebec City*

The joint frequency distributions for the surface wind directions versus the above-valley wind directions for Quebec City as a function of season are plotted in Fig. 9. Similar to that of Fig. 8, the solid (dashed) lines represent axes that are parallel (normal) to the mean axis of the SLRV at Quebec City. From the joint frequency distribution plots in Fig. 9 it is clear that the pressure-driven channeling wind regime is dominant at YQB. The strong bidirectionality and channeling of the surface winds is clearly apparent as surface wind directions remain relatively constant for a broad range of 925-hPa geostrophic wind directions. The dramatic shift (~180°) of the surface winds across the 230° geostrophic wind direction axis, which is parallel to the axis of the SLRV, is clearly apparent. This classic pressure-driven channeling signature is present throughout all seasons.

The diagonal line plotted in Fig. 9 represents the axis for the downward momentum transport mechanism. We noted that this mechanism was important at YUL for geostrophic wind directions ranging from 240° to 340°. For the downward momentum transport we would expect the surface wind directions to increase as the geostrophic wind directions increase (i.e., lie parallel to the diagonal line). At YQB this mechanism is not as prominent. For geostrophic wind directions ranging from 240° to 360° the surface wind directions remain relatively constant.

Countercurrents are also present at YQB, most prominent in the winter, spring, and fall seasons (Figs. 9a,b,d). In particular, the local maximum in surface wind directions centered near 70° is associated with 925-hPa geostrophic wind directions concentrated between 160° and 220°. Hence we have a northeasterly surface wind, when projected into the SLRV, which is accompanied by a southwesterly above-valley geostrophic wind component, when projected into the SLRV.

### c. Burlington

The joint frequency distributions of the surface wind directions versus the above-valley wind directions as a function of season for BTV are shown in Fig. 10. As noted in section 3, the predominance of surface southerly and northerly winds at Burlington is clearly seen in the joint frequency distribution plots. For geostrophic wind directions between 300° and 360°, downward momentum transport appears to be present in all seasons. There is a distinct shift in the surface wind directions as the geostrophic wind directions cross the 270° axis (see Figs. 10a–d), which is normal to the mean position of the LCV axis. The surface wind directions shift from 160°–170° to 320°–330°, which is a characteristic of the forced channeling mechanism. Countercurrents do not appear to be present at BTV.

We did not see strong evidence for the presence of the thermal forcing mechanism at YUL or YQB (not shown), however at BTV, which is situated to the east of Lake Champlain (Fig. 2), diurnal thermal forcing does appear to be important during the JJA season. Figure 11 shows the joint frequency distribution of the surface wind directions versus the above-valley wind directions for BTV as a function of time of day. Examining Fig. 11 we note that while the surface wind maximum centered at 170° is present throughout the day, there is a preference for surface winds in the 270° (westerly)–360° (northerly) sector in the late morning and afternoon hours (1500–0000 UTC; Figs. 11a,f,g,h). In the late evening and early morning hours (0300–0900 UTC; Figs. 11b–e) there is a preference for surface winds in the 40° (northeasterly)–100° (easterly) sector. These diurnal directional surface wind shifts are consistent with the location of Lake Champlain to the west of BTV and appear to be independent of the 925-hPa geostrophic wind directions (see Fig. 11). Furthermore these diurnal surface wind direction shifts are most prominent when the 925-hPa geostrophic winds are weak (not shown).

## 5. Discussion

In this section we elaborate and expand our discussion of the results presented in section 4. It should be emphasized that the wind climatology at a particular valley location is often complex, resulting from a combination of physical processes. This makes interpretations somewhat difficult. At Montreal (see Fig. 2), the physiography of the SLRV is complex, as the valley broadens considerably and the close proximity of the LCV to the south and the Ottawa River Valley to the west (see Fig. 2a) would be expected to influence local wind conditions. In particular, if we refer back to Fig. 8, the secondary mode or maximum in surface southeasterly wind directions (130°–180°), which is present in all seasons (Fig. 3), occurs preferentially with 925-hPa geostrophic wind directions concentrated in the southwesterly wind direction quadrant (180°–260°). These southeasterly surface winds are not aligned along the axis of the SLRV and are most prominent during the SON period (Figs. 3d, 8d). We suggest that these southeasterly surface winds result from outflow fanning from the LCV.

To examine this issue we focus upon the SON time period, when southeasterly surface winds at YUL are most frequent, and isolate events of persistent southeasterly surface winds. Events are defined as time periods of 12 h or greater where the surface wind directions at YUL are consistently between 140° and 170°. In total we identified 111 cases for the SON period from 1979 to 2002. For these same events, we examined the surface wind directions at BTV. In Fig. 12a we have plotted the distribution of surface wind directions at BTV for the persistent southeasterly wind events at YUL. Over two-thirds of the time surface winds at BTV are from 160°–180°, southerly channeled winds. The corresponding sea level pressure field, taken from the NARR, averaged over the 111 southeasterly wind events, is shown in Fig. 12b. The SLP field is dominated by an anticyclone located off the east coast of Nova Scotia, Canada, and a meridionally orientated cyclone located over Hudson Bay. This SLP pattern is typically observed during periods of forced wind channeling within the LCV (J. Goff, NWS, 2008, personal communication).

The southeasterly surface winds observed at YUL are somewhat ageostrophic and appear to have a pressure-driven component with the synoptic-scale low (high) pressure situated to the northwest (southeast). Studies of atmospheric flows at the exit region of gaps indicate that the dynamics of the flow can be quite different when compared to the flow within the gap (Overland 1984; Steenburgh et al. 1998; Colle and Mass 2000; Gaberšek and Durran 2006). In particular, studies have shown the presence of diffluent flow at the exit region of gaps that can extend a considerable distance downstream (Steenburgh et al. 1998; Colle and Mass 2000; Chelton et al. 2000). A detailed study of this outflow fanning region would require high-resolution modeling, which is beyond the scope of the current paper.

Our analysis in section 4 indicated that pressure-driven channeling was prominent at both YUL and YQB within the SLRV, but that forced channeling was prominent at BTV. Numerous studies have alluded to the importance of the local terrain details, such as valley orientation, length, width, and depth in determining the dominance of one forcing mechanism over another (Weber and Kaufmann 1998; Bergström and Juuso 2006;

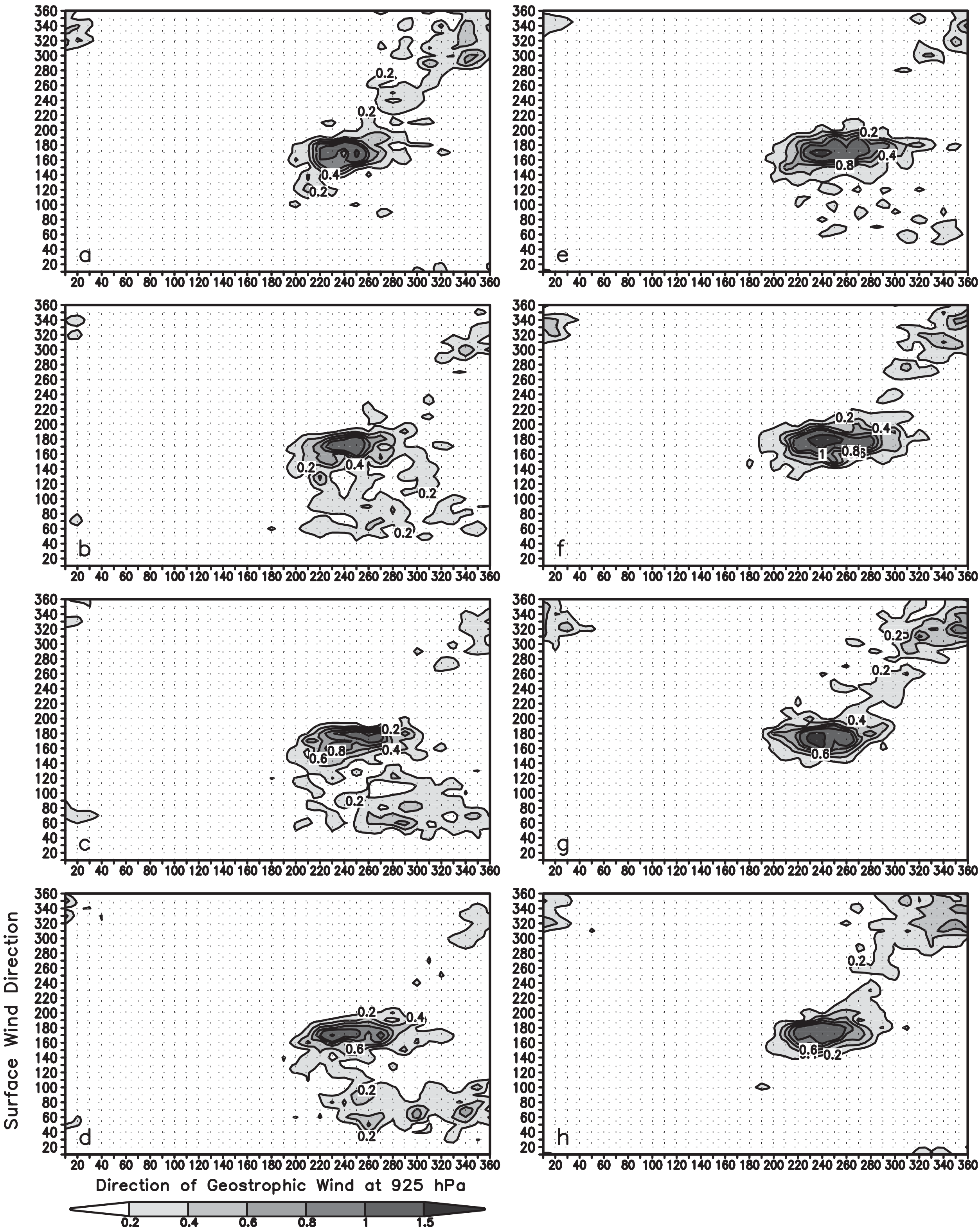


FIG. 11. Joint frequency distributions of surface wind directions (ordinate) vs 925-hPa geostrophic wind directions (abscissa) for BTV for JJA 1979–2002: (a) 0000, (b) 0300, (c) 0600, (d) 0900, (e) 1200, (f) 1500, (g) 1800, and (h) 2100 UTC.

Nawri and Stewart 2008). Weber and Kaufmann (1998) in their study of synoptic-scale influences on local wind conditions in the complex terrain near Basel, Switzerland, during the Modell für Immissions-Schutz bei Transport und Ausbreitung von Luftfremdstoffen (MISTRAL) field experiment noted a critical relationship between valley width and depth that appears to govern whether pressure-driven channeling or forced channeling tends to dominate. In particular, the authors found that narrow valleys with widths on the order of 2–3 km appeared to favor the forced channeling mechanism, while wider valleys with widths in the range of 6–10 km were governed by pressure-driven channeling (Weber and Kaufmann 1998).

The width and depth relationships for the SLRV and the LCV valleys in the vicinities of YQB and BTV do not appear to be significantly different (see Fig. 2). The LCV, in the vicinity of BTV, is seen to be narrower than the SLRV near YQB, which would be consistent with the predominance of forced channeling at BTV. Orographic features of a particular site are undoubtedly important in determining the dominance of one physical mechanism over another, however we have not investigated this aspect in greater detail. Instead, to provide further insight into why pressure-driven channeling dominates at YUL and YQB and forced channeling at BTV, we examine events of pressure-driven channeling at YUL in more detail. Using a similar methodology used to isolate southeasterly wind events at YUL, northeasterly wind events at YUL represent 12-h periods or greater where the surface wind directions are consistently in the 30°–50° range. For the DJF 1979–2002 period we have identified 151 such events, with the time-mean SLP field plotted in Fig. 12c.

The time-mean SLP field, calculated from the NARR, is dominated by a low pressure center situated over Lake Erie and a high pressure center situated in northern Quebec (Fig. 12c). This cyclone–anticyclone couplet is similar to the persistent SLP distribution during the ice storm of 1998 (Gyakum and Roebber 2001; Roebber and Gyakum 2003) and is similar to the composite SLP field associated with freezing rain events over the eastern region of the Great Lakes found by Cortinas (2000). The SLP gradient is maximized along the mean axis of the SLRV and is consistent with pressure-driven northeasterly surface winds at YUL.

Also plotted in Fig. 12c is the time-averaged lower-tropospheric vertical temperature gradient, as represented by the temperature difference at 850 and 1000 hPa from the NARR, for the persistent northeasterly surface wind events at YUL. Note that the NARR assimilates rawinsonde temperatures and hence we expect the analysis of upper-air temperatures to be quite accurate (Mesinger et al. 2006). The section of the SLRV that extends southwest from YQB past YUL and terminates in eastern Ontario is statically stable with a time-mean lower-tropospheric temperature inversion. As further verification, for all 0000 and 1200 UTC times during events of persistent surface northeasterly winds at YUL, we calculated the temperature differences between the NARR 850-hPa temperatures, interpolated to the location of YUL, and the surface temperatures reported at YUL. A total of 287 temperature differences was calculated, with a mean difference of 2.12°C and over two-thirds of the temperature differences being positive. Temperature data from the rawinsonde site located at Maniwaki, Canada (WMW), whose location is shown in Fig. 12c, are consistent with the above findings. The presence of the lower-tropospheric temperature inversion acts to decouple the surface winds from those at ridge level and allows the valley winds at YUL and YQB to respond directly to the synoptic-scale pressure gradient.

For comparison purposes, we have isolated events of southerly channeled flow at BTV for the SON 1979–2002 period. These events represent 12-h periods or greater with surface wind directions between 160° and 180°. A total of 211 events were identified, with the time-averaged SLP and lower-tropospheric vertical temperature gradient shown in Fig. 12d. The SLP distribution looks similar to that shown in Fig. 12b with a large-scale ridge of high pressure situated to the south of the Canadian Maritimes and a trough axis centered over the Great Lakes region. The time-averaged lower-tropospheric vertical temperature gradients indicate an atmosphere that is well mixed in the vicinity of BTV (Fig. 12d). For all 0000 and 1200 UTC times during southerly channeled flow events at BTV we calculated the temperature difference between the NARR 850-hPa temperatures interpolated to the location of BTV and the surface temperatures reported at BTV. A total of 367 temperature differences were calculated, with a mean temperature difference of −5.5°C. A total of 20, or roughly 5%, of the temperature differences were associated with a lower-tropospheric temperature inversion. The presence of the well-mixed lower troposphere is consistent with the forced channeling mechanism, and differs considerably from the lower-tropospheric conditions during northeasterly channeled flow within the SLRV during the DJF period.

## 6. Conclusions

In this study we have examined the long-term surface wind climatology of the SLRV and the LCV in an effort to document the physical mechanism(s) responsible for the channeling of the surface winds. This was accomplished

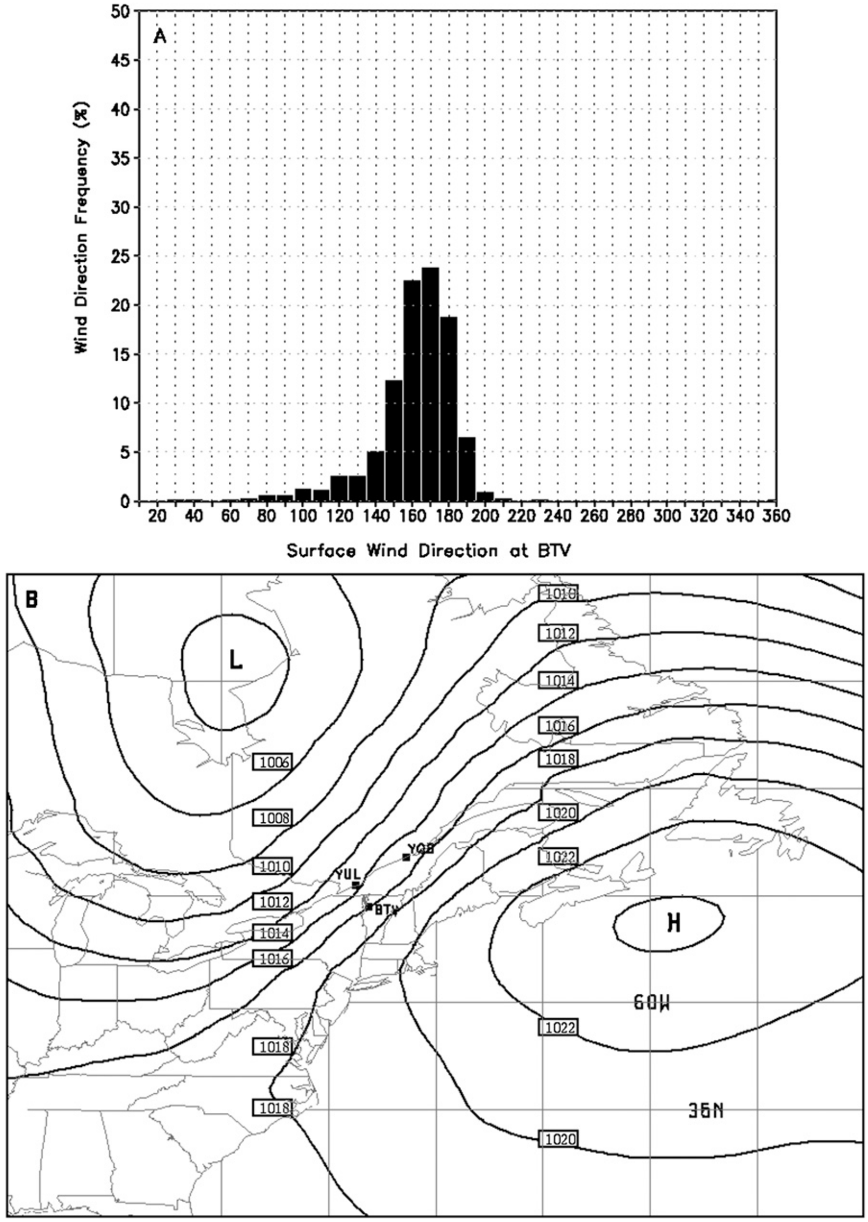


FIG. 12. (a) Histogram representing the distribution of surface wind directions at BTV during events of persistent southeasterly winds at YUL. SLP (hPa) for (b) persistent southeasterly flow events at YUL during SON 1979–2002 (111 events), and temperature differences between 850 and 1000 hPa (°C) for (c) persistent northeasterly flow events at YUL during DJF 1979–2002 (151 events) and (d) persistent southerly flow events at BTV during SON 1979–2002 (211 events). The locations of the three meteorological stations are shown in (b),(c), and (d). The location of the upper-air rawinsonde station at WMW is shown in (c).

using three representative stations within the SLRV and the LCV over the relatively long, 24-yr period. We are not aware of any other such study of the long-term surface wind climatology within the SLRV or the LCV.

An analysis of the surface wind distributions at Montreal (YUL), Quebec City (YQB), and Burlington, Vermont (BTV), revealed strong bidirectionalities in the surface wind directions. At YQB the bidirectionality is extremely pronounced throughout the year, owing to the channeling effects of the SLRV. At BTV, the prominent wind direction throughout all seasons is southerly. The 925-hPa geostrophic wind directions for all localities had a predominant westerly component, with the strongest winds during the winter season.

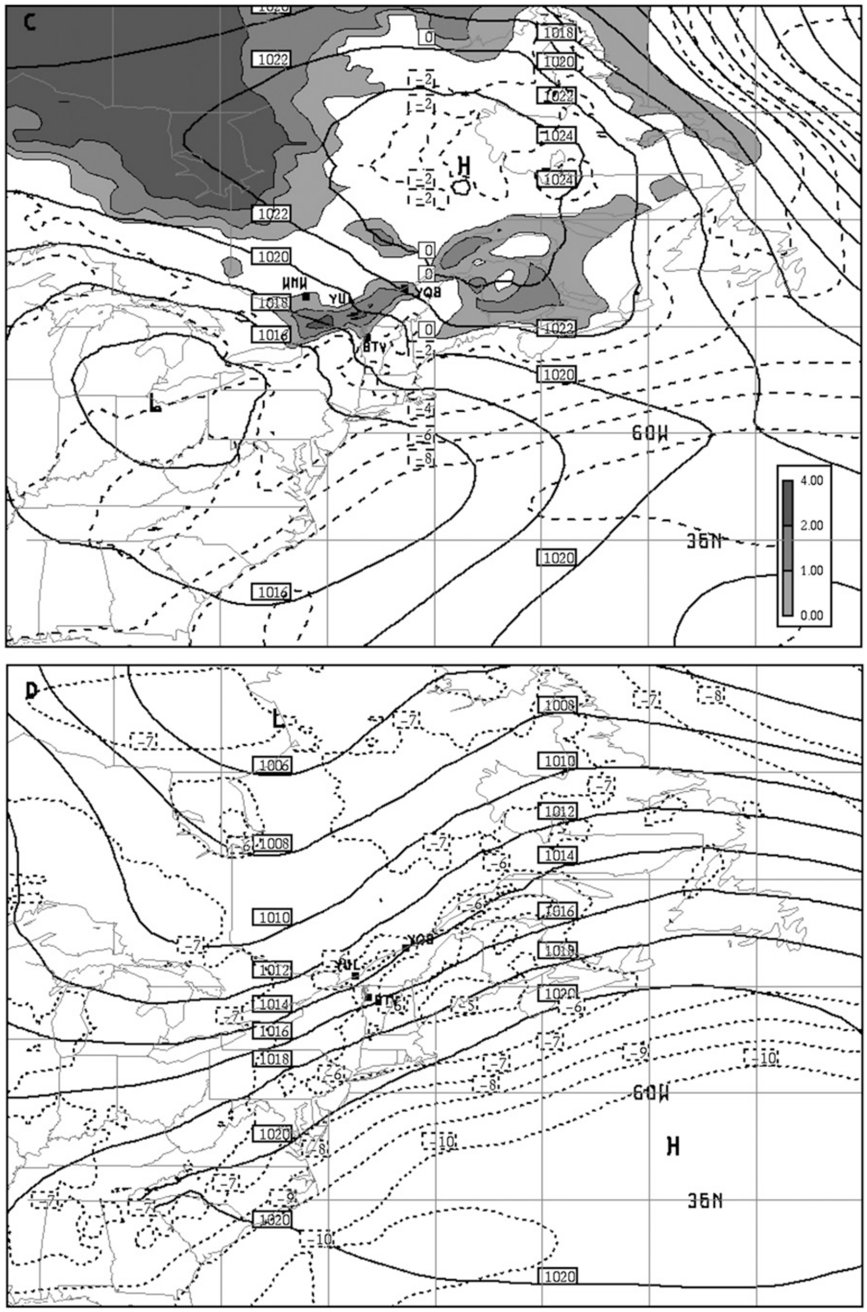


FIG. 12. (*Continued*)

Our study of the physical mechanisms responsible for the pronounced channeling of the surface winds focused upon four mechanisms within the context of the classical mechanisms described by Whiteman and Doran (1993): thermally driven channeling, downward momentum transport, forced channeling, and pressure-driven channeling. Each of these physical mechanisms possesses a unique signature in the joint frequency distribution plots of the valley wind directions versus the ambient wind directions. The wind climatology of a given station is often the result of varying contributions from these four mechanisms.

At YUL, downward momentum transport was found to be prominent for 925-hPa geostrophic wind directions ranging from 240° to 340° (i.e., southwesterly to northwesterly). For this range of 925-hPa geostrophic wind directions the surface winds tended to be shifted roughly 25° toward lower pressure (Fig. 8). Pressure-driven channeling is the dominant mechanism producing northeasterly surface winds at YUL. These northeasterlies are most prominent in the winter, spring, and fall seasons. The existence of countercurrents at YUL in association with surface northeasterlies was shown to be present during the winter, spring, and fall seasons.

Plots of the joint frequency distributions of valley wind directions versus ambient wind directions as a function of season for YQB indicated clearly that pressure-driven channeling is the dominant mechanism responsible for the channeling of surface winds. The dramatic shift (~180°) of the surface winds across the 230° geostrophic wind direction axis is clearly apparent throughout all seasons. Downward momentum transport was not found to be especially prominent at YQB. Similar to YUL, countercurrents associated with surface northeasterlies are present at YQB.

The pressure-driven channeling along the SLRV, documented by Roebber and Gyakum (2003) as important to the longevity and severity of the 1998 ice storm, was placed into a climatological context by showing that northeasterly surface winds at Montreal are predominantly pressure driven, while the channeling of surface winds at Quebec City are fundamentally pressure driven throughout the year. Forced channeling was found to be present at BTV throughout all seasons. A distinct shift in surface wind directions across the 270°, 925-hPa geostrophic wind direction axis was apparent. Unlike YUL and YQB, the proximity of Lake Champlain results in diurnal thermal forcing of the surface winds during the JJA season under weak 925-hPa geostrophic wind environments.

Examination of individual channeling events within the SLRV and the LCV indicated that for channeling events within the SLRV the enhanced atmospheric stability in terms of the presence of a lower-tropospheric temperature inversion is important in decoupling the surface winds from the upper-level geostrophic winds and allowing the surface winds to respond directly to the along-valley pressure gradient. Channeling events within the LCV were found to occur under lower-tropospheric atmospheric conditions that were well mixed, favoring the forced channeling mechanism. Laird et al. (2009) in their study of lake effect precipitation found the lower-tropospheric environment over Lake Champlain to be well mixed, suggesting that the modified environment was likely the result of the isolating nature of the LCV.

It is important to address the limitations of this study. The focus of this study was the characterization of surface wind channeling within both the SLRV and the LCV within the context of the classical mechanisms discussed by Whiteman and Doran (1993). These physical mechanisms are not mutually exclusive and additional physical insight into the surface wind channeling mechanisms would require an enhanced mesoscale observing network, including radiosondes and dropsondes, aircraft in situ measurements, and Doppler radar wind scanning. Based upon the experience and knowledge gained from the Dynamics of Gap Flow (GAP) subproject of MAP, Mayr et al. (2007) discuss in detail the observational and high-resolution modeling requirements for future studies. In particular, the authors emphasize the need for high temporal and spatial resolution sampling of the vertical structure of the upstream and downstream reservoirs along the gap or channel.

Given the importance of countercurrents and their potential linkage with extreme weather, future work will examine individual events of countercurrents at both YUL and YQB. Preliminary work has indicated that events of countercurrents with northeasterly surface winds at YUL and YQB are associated with a distinct signature in the large-scale pressure field with the presence of the cyclone–anticyclone couplet that Gyakum and Roebber (2001) discussed.

*Acknowledgments.* The North American Regional Reanalysis (NARR) data for this study were provided by the National Climatic Data Center and we acknowledge their support. The authors thank Mr. Paul Sisson for providing the hourly wind and temperature data for Burlington, Vermont. Insightful discussion with Dr. Eyad Atallah and the comments and suggestions of two anonymous reviewers led to an improved manuscript. This research has been supported in part by grants from the Natural Sciences and Engineering Research Council (NSERC) and Mathematics of Information Technology and Complex Systems (MITACS). We acknowledge the support of the Ouranos Consortium.

REFERENCES

Bergström, H., and N. Juuso, 2006: A study of valley winds using the MIUU meso-scale model. *Wind Energy,* **9,** 109–129.

Chelton, D. B., M. H. Freilich, and S. K. Esbensen, 2000: Satellite observations of the wind jets off the Pacific Coast of Central America. Part II: Regional relationships and dynamical considerations. *Mon. Wea. Rev.,* **128,** 2019–2043.

Cohn, S., J. R. Gyakum, R. R. Rogers, W. L. Ecklund, D. A. Carter, and J. S. Wilson, 1996: Wind profiler/RASS observations of two complex synoptic events. *Beitr. Phys. Atmos.,* **69,** 37–47.

Colle, B. A., and C. F. Mass, 1998: Windstorm along the western side of the Washington Cascade Mountains. Part I: A high-resolution observational and modeling study of the 12 February 1995 event. *Mon. Wea. Rev.,* **126,** 28–52.

——, and ——, 2000: High-resolution observations and numerical simulations of easterly gap flow through the Strait of Juan de Fuca on 9–10 December 1995. *Mon. Wea. Rev.,* **128,** 2398–2422.

Cortinas, J., Jr., 2000: A climatology of freezing rain in the Great Lakes region of North America. *Mon. Wea. Rev.,* **128,** 3574–3588.

——, B. C. Bernstein, C. C. Robbins, and J. W. Strapp, 2004: An analysis of freezing rain, freezing drizzle, and ice pellets across the United States and Canada: 1976–90. *Wea. Forecasting,* **19,** 377–390.

Drobinski, P., and Coauthors, 2007: Fohn in the Rhine Valley during MAP: A review of its multiscale dynamics in complex valley geometry. *Quart. J. Roy. Meteor. Soc.,* **133,** 897–916.

Eckman, R. M., 1998: Observations and numerical simulations of winds within a broad forested valley. *J. Appl. Meteor.,* **37,** 206–219.

Fitzjarrald, D. R., and C. G. Lala, 1989: Hudson Valley fog environments. *J. Appl. Meteor.,* **28,** 1303–1328.

Gaberšek, S., and D. R. Durran, 2006: Gap flows through idealized topography. Part II: Effects of rotation and surface friction. *J. Atmos. Sci.,* **63,** 2720–2739.

Gross, G., and F. Wippermann, 1987: Channeling and countercurrent in the upper Rhine Valley: Numerical simulations. *J. Climate Appl. Meteor.,* **26,** 1293–1304.

Gyakum, J. R., and P. J. Roebber, 2001: The 1998 ice storm—Analysis of a planetary-scale event. *Mon. Wea. Rev.,* **129,** 2983–2997.

Kossmann, M., and A. P. Sturman, 2003: Pressure-driven channeling effects in bent valleys. *J. Appl. Meteor.,* **42,** 151–158.

Lackmann, G. M., and J. E. Overland, 1989: Atmospheric structure and momentum balance during a gap-wind event in Shelikof Strait, Alaska. *Mon. Wea. Rev.,* **117,** 1817–1833.

Laflamme, J. N., and G. Périard, 1998: The climate of freezing rain over the province of Quebec in Canada: A preliminary analysis. *Atmos. Res.,* **46,** 99–111.

Laird, N. F., J. Desrochers, and M. Payer, 2009: Climatology of lake-effect precipitation events over Lake Champlain. *J. Appl. Meteor. Climatol.,* **48,** 232–250.

Mayr, G. J., and Coauthors, 2004: Gap flow measurements during the Mesoscale Alpine Programme. *Meteor. Atmos. Phys.,* **86,** 99–119.

——, and Coauthors, 2007: Gap flows: Results from the Mesoscale Alpine Programme. *Quart. J. Roy. Meteor. Soc.,* **133,** 881–896.

Mesinger, F., and Coauthors, 2006: North American Regional Reanalysis. *Bull. Amer. Meteor. Soc.,* **87,** 343–360.

Nawri, N., and R. E. Stewart, 2006: Climatological features of orographic low-level jets over Frobisher Bay. *Atmos.–Ocean,* **44,** 397–413.

——, and ——, 2008: Channeling of high-latitude boundary-layer flow. *Nonlinear Processes Geophys.,* **15,** 33–52.

Neiman, P. J., F. M. Ralph, A. B. White, D. D. Parrish, J. S. Holloway, and D. L. Bartels, 2006: A multiwinter analysis of channeled flow through a prominent gap along the Northern California coast during CALJET and PACJET. *Mon. Wea. Rev.,* **134,** 1815–1841.

Overland, J. E., 1984: Scale analysis of marine winds in straits and along mountain coasts. *Mon. Wea. Rev.,* **112,** 2530–2534.

Payer, M., J. Desrochers, and N. F. Laird, 2007: A lake-effect snow band over Lake Champlain. *Mon. Wea. Rev.,* **135,** 3895–3900.

Powe, N. N., 1968: The influence of a broad valley on the surface winds within the valley. Canadian Department of Transport, Meteorology Bureau Rep. TEC-668, 9 pp. [Available from the Canadian Government Publishing Centre, Supply and Services Canada, Ottawa, ON K1Z 0S9, Canada.]

Rampanelli, G., D. Zardi, and R. Rotunno, 2004: Mechanisms of up-valley winds. *J. Atmos. Sci.,* **61,** 3097–3111.

Reid, S., 1996: Pressure gradients and winds in Cook Strait. *Wea. Forecasting,* **11,** 476–488.

Roebber, P. J., and J. R. Gyakum, 2003: Orographic influences on the mesoscale structure of the 1998 ice storm. *Mon. Wea. Rev.,* **131,** 27–50.

Sharp, J., and C. Mass, 2002: Columbia Gorge gap flow. *Bull. Amer. Meteor. Soc.,* **83,** 1757–1762.

Slonosky, V. C., 2003: The meteorological observations of Jean-Francois Gaultier, Quebec, Canada: 1742–56. *J. Climate,* **16,** 2232–2247.

Steenburgh, W. J., D. M. Schultz, and B. A. Colle, 1998: The structure and evolution of gap outflow over the Gulf of Tehuantepec, Mexico. *Mon. Wea. Rev.,* **126,** 2673–2691.

Stewart, J. Q., C. D. Whiteman, W. J. Steenburgh, and X. Bian, 2002: A climatological study of thermally driven wind systems of the U.S. Intermountain West. *Bull. Amer. Meteor. Soc.,* **83,** 699–708.

Stuart, R., and G. Isaac, 1999: Freezing precipitation in Canada. *Atmos.–Ocean,* **37,** 87–102.

Weber, R. O., and P. Kaufmann, 1998: Relationship of synoptic winds and complex terrain flows during the MISTRAL field experiment. *J. Appl. Meteor.,* **37,** 1486–1496.

Whiteman, D. C., and J. C. Doran, 1993: The relationship between overlying synoptic-scale flows and wins within a valley. *J. Appl. Meteor.,* **32,** 1669–1682.

Zhong, S., J. Li, C. D. Whiteman, X. Bian, and W. Yao, 2008: Climatology of high wind events in the Owens Valley, California. *Mon. Wea. Rev.,* **136,** 3536–3552.